

Polarization Effects in Laser-Assisted (e,2e) Collision on H-atom by Twisted Electrons

Neha* and Rakesh Choubisa†

*Department of Physics, Birla Institute of Technology and Science,
Pilani, Pilani Campus, Vidya Vihar, Pilani, Rajasthan 333031, India*

(Dated: March 4, 2026)

The dynamics of fast (e, 2e) collisions, induced by the impact of twisted electron beams, on atomic hydrogen, is analyzed in the presence of a laser field with circular and linear polarization. For the (e,2e) differential cross-section calculations we use Volkov and Coulomb-Volkov wave functions for scattered and ejected electrons, respectively, while the laser-atom interaction is treated in first-order perturbation theory. The formalism is developed for the asymmetric coplanar geometry in the first Born approximation. We investigate the influence of laser field polarization and provide a comparative analysis of Triple Differential Cross-Section's (TDCS) for circularly and linearly polarized laser fields as a function of ejected electron angle. The overall magnitude of the cross-section is larger for circular polarization as compared to linear polarization. Some notable changes in the angular distributions of TDCS were also observed for the circular polarization as compared to that for linear polarization. We further extend the study to coherent superpositions of twisted electron beams to examine OAM effects for macroscopic target which shows that the $TDCS_{av}$ is strongly sensitive to the difference of the projectile's OAM as well as on the phase difference between them.

I. INTRODUCTION

The study of microscopic target ionization induced by electron impact, commonly known as the (e,2e) process, provides valuable insight into the electronic structure of the atomic target and the resulting residual ion [1]. Understanding of the electronic structure of microscopic targets is essential for modeling and analyzing laboratory plasmas, astrophysical processes, laser dynamics, and fields such as chemistry and biology [2–5]. The field-free experimental studies have been conducted on various atomic targets [6–8].

With the rapid development of laser technology and significant advances in multiparticle detection techniques, the study of laser-assisted electron–atom collision processes has attracted considerable experimental and theoretical interest. Electron-impact ionization of atoms in the presence of a laser field is commonly referred to as the laser-assisted (e,2e) collision [9]. The laser-assisted electron-impact ionization experimental study was conducted on helium [10, 11]. Several theoretical studies of triple differential cross-sections in different kinematical arrangements provide a general understanding of these phenomena [9, 12–14]. Initial studies of laser-assisted ionization processes did not account for the dressing effects of the target; however, these effects were included in the final state by representing them as Volkov or Coulomb-Volkov states [15–21]. Joachain and his colleagues were the first to account for the dressing effects of the target due to the laser field [22, 23]. They observed significant variations in the angular distributions of the differential cross-section. Numerous theoretical analyses on laser-assisted single and double ionization of atomic targets have been reported in the literature [24–32]. Taïeb et al. [31] and Makhoute et al. [30] investigated the effects of laser polarization, specifically linear polarization (LP) and circular polarization (CP_Y), on the laser-assisted (e, 2e) process on hydrogen and helium, respectively. Their studies focused on angular distribution of TDCS as a function of ejected electron in an asymmetric coplanar geometry and demonstrated that a CP_Y laser produces a significantly larger TDCS compared to that for the LP lasers. These studies have opened new avenues for both theoretical and experimental research in this field. However, the reported studies were carried out using conventional electron beams described by plane waves, which do not carry orbital angular momentum.

However, in the last few decades, the production of new structured light known as “vortex beam or twisted beam” has led to a renewed interest in (e,2e) collisions for atomic and molecular targets [33–42]. In particular, vortex beams have many properties that make them quite different from conventional plane waves. For example, a “vortex electron beam” or a “twisted electron beam” (TEB) carries quantized orbital angular momentum (OAM) along the propagation direction and has non-zero transverse linear momentum [43]. The quantized OAM of TEB is a characteristic of the helical wavefronts possessed by the TEB [44–46]. The distinctive properties of twisted electron beams (TEBs), like orbital angular momentum and structured wavefront, provide new possibilities for fundamental studies and applications in

*Electronic address: p20210062@pilani.bits-pilani.ac.in

†Electronic address: rchoubisa@pilani.bits-pilani.ac.in

areas such as high-resolution imaging, quantum state manipulation, optical trapping, information transfer, astronomy, and high-order harmonic generation [46–52]. Collision physics, with its long-standing role in revealing fundamental aspects of atomic and molecular structure and few-body interactions, offers essential insights for understanding how structured electrons interact with matter. The above-discussed studies have been conducted for the field-free case. Our study aims to see the impact of the presence of a laser field in asymmetric coplanar geometries. In our previous work [53], we investigated the laser assisted ($e, 2e$) ionization of atomic hydrogen induced by twisted electron beams in the presence of a linearly polarized laser field. In that study, the influence of the orbital angular momentum carried by the incident electron on the Triple Differential Cross Section (TDCS) was analyzed under well-defined kinematical conditions. Previous investigations of laser-assisted ($e, 2e$) processes with plane-wave projectiles [30, 31] have reported angular distributions characterized by a dominant binary peak and a weaker, broadened recoil peak. These studies further showed that circularly polarized laser fields generally produce larger TDCS than that for linear polarization. This enhancement has been associated with the distinct symmetry properties and interaction dynamics introduced by circular polarization. The motivation of the present work is to extend our previous analysis to the case of circular polarization to examine whether the enhancement of the TDCS observed for circularly polarized fields persists when the incident electron is described by a twisted (vortex) wavefunction carrying orbital angular momentum. In addition to this we would like to compare the TDCS for the linearly and circularly polarised. To provide a more experimentally relevant description, we also examine TDCS for the coherent superpositions of twisted electron beams, which enable a systematic investigation of the orbital angular momentum (OAM) effect on the TDCS. This allows us to explore how the phase structure of structured projectiles alters the collision dynamics during the laser-assisted ionization.

The paper is organized as follows: In Section II, we present our theoretical model, which is employed to study the laser-assisted ($e, 2e$) process for both plane wave and twisted electron beam impacts. In section III we discuss our theoretical formalism. Section IV presents our conclusions.

Throughout the paper, atomic units are used unless stated otherwise.

II. THEORETICAL FORMALISM

A. Plane wave ($e, 2e$) on H-atom

The theoretical framework employed in the present work follows closely our earlier formulation developed for the laser-assisted ($e, 2e$) ionization of atomic hydrogen induced by twisted electron beams in a linearly polarized laser field. In the present study, the formalism is extended to the case of a circularly polarized laser field, while the treatment of the twisted projectile and the target interaction remains unchanged.

The basic laser-assisted ($e, 2e$) process accompanied by the absorption or emission of l photons from the laser field can be described by the following equation:

$$e^-(\mathbf{k}_i) + H + l\omega \rightarrow H^+ + e^-(\mathbf{k}_s) + e^-(\mathbf{k}_e) \quad (1)$$

Here, \mathbf{k}_i , \mathbf{k}_s and \mathbf{k}_e incident momentum, scattered and ejected electron momentum respectively. l is the number of photons exchanged between the laser-field and the atom-projectile system and ω is the photon energy. In this study, we consider the laser field circularly polarised (CP) and treat it classically within the dipole approximation which means that it varies little over the atomic range. The vector potential of a CP field propagating along the \hat{z} -axis:

$$\mathbf{A}(t) \rightarrow A_0(\hat{x} \cos(\omega t) + \hat{y} \sin(\omega t) \tan(\eta/2)) \quad (2)$$

the corresponding monochromatic electric field is:

$$\mathbf{E}(t) \rightarrow E_0(\hat{x} \sin(\omega t) - \hat{y} \cos(\omega t) \tan(\eta/2)) \quad (3)$$

where $\mathbf{E}_0 = \mathbf{A}_0 \omega/c$ where, E_0 is the field strength, ω is the laser frequency, and c is the speed of light. Here η presents the degree of ellipticity. Linear polarization corresponds to $\eta = 0$ and circular polarization corresponds to $\eta = \pi/2$. The main aim of this study is to calculate the transition matrix element (T_{fi}) in the first Born approximation (FBA) for the transition from the initial state ψ_i to the final state ψ_f . For the laser-assisted ($e, 2e$) process the transition matrix element in the first Born approximation is given as [22]:

$$T_{fi}^{B1} = -i \int_{-\infty}^{+\infty} dt \left\langle \chi_{k_s}(\mathbf{r}_0, t) \Phi_{k_e}(\mathbf{r}_1, t) \left| \frac{-1}{r_0} + \frac{1}{|\mathbf{r}_0 - \mathbf{r}_1|} \right| \chi_{k_i}(\mathbf{r}_0, t) \Phi_0(\mathbf{r}_1, t) \right\rangle \quad (4)$$

In equation (4), \mathbf{r}_0 is the position vector of the incident (and scattered) electron, \mathbf{r}_1 represents the coordinates of the bound electron of the target. In equation (4) χ_{k_i} and χ_{k_s} are the Volkov wavefunctions of the incident and

scattered electron for the non-relativistic motion in circularly polarised laser-field and is described as [30] :

$$\chi_{\mathbf{k}}(\mathbf{r}_0, t) = (2\pi)^{-3/2} \exp\{i(\mathbf{k} \cdot \mathbf{r}_0 - E_k t - \Delta_k \sin(\omega t - \gamma_k))\} \quad (5)$$

where, the effect of circularly polarised field is included by the term Δ_k , given by equation (7):

$$\Delta_k = \alpha_0((\mathbf{k} \cdot \hat{\mathbf{x}})^2 + (\mathbf{k} \cdot \hat{\mathbf{y}})^2 \tan^2\left(\frac{\eta}{2}\right)) \quad (6)$$

and

$$\tan(\gamma_k) = \frac{\mathbf{k} \cdot \hat{\mathbf{y}}}{\mathbf{k} \cdot \hat{\mathbf{x}}} \tan\left(\frac{\eta}{2}\right) \quad (7)$$

The dressed state of the ejected electron in the continuum state under the influence of combined field of the residual ion and the external circularly polarised laser field, proposed by Joachain et al., [22] can be written as :

$$\begin{aligned} \Phi_{k_e}^{(-)}(\mathbf{r}_1, t) = & e^{-i\mathbf{a} \cdot \mathbf{r}_0} e^{-iE_{k_e} t} e^{-i\Delta_{k_e} \sin(\omega t - \gamma_{k_e})} \left\{ \psi_{C, k_e}^{(-)}(\mathbf{r}) [1 + i\Delta_{k_e} \sin(\omega t - \gamma_{k_e})] \right. \\ & \left. + \frac{i}{2} \sum_n \left[\frac{e^{i\omega t}}{E_n - E_{k_e} + \omega} - \frac{e^{-i\omega t}}{E_n - E_{k_e} - \omega} \right] M_{nj} \psi_n(\mathbf{r}) \right\} \end{aligned} \quad (8)$$

with

$$M_{nj} = \langle \psi_n | \boldsymbol{\varepsilon} \cdot \mathbf{r}_i | \psi_{k_e} \rangle \quad (9)$$

Here $\psi_{C, k_e}^-(r_1)$ is the Coulomb wave function, and $\boldsymbol{\varepsilon} = (\hat{\mathbf{e}}_x + i\hat{\mathbf{e}}_y)/\sqrt{2}$ represents the polarization vector of the circularly polarized electric field, where $\hat{\mathbf{e}}_x$ and $\hat{\mathbf{e}}_y$ denote unit vectors along two mutually orthogonal directions in the polarization plane.

Using wave functions of target, incident, scattered, and ejected electrons in the first Born T -matrix element ((4)) and integrating over time, we obtain T_{fi}^{B1} for the circularly polarized light as:

$$T_{fi}^{B1} = (2\pi)^{-1} i \sum_{l=-\infty}^{+\infty} \delta(E_{k_s} + E_{k_e} - E_{k_i} - E_0 - l\omega) e^{il\gamma} f_{ion}^{B1, l} \quad (10)$$

where

$$\tan(\gamma) = \frac{-\Delta_{k_s} \sin(\gamma_{k_s}) + \Delta_{k_e} \sin(\gamma_{k_e}) - \Delta_{k_i} \sin(\gamma_{k_i})}{\Delta_{k_s} \cos(\gamma_{k_s}) + \Delta_{k_e} \cos(\gamma_{k_e}) + \Delta_{k_i} \cos(\gamma_{k_i})} \quad (11)$$

Within the first Born approximation, the scattering amplitude $f_{ion}^{B1, l}$ describes the laser-assisted ionization process accompanied by the net exchange of l photons between the atomic system and the external circularly polarized laser field. Following the formalism of Ref. [22], this amplitude naturally decomposes into three distinct contributions, reflecting the different interaction pathways induced by the presence of the circularly polarized electromagnetic field. In the following equations, we rewrite the decomposed form of the scattering amplitude for the circularly polarised field:

$$f_{ion}^{B1, l} = f_I + f_{II} + f_{III}. \quad (12)$$

where,

$$f_I = -2\Delta^{-2} J_l(\lambda) \left\langle \psi_{C, k_e}^- | \exp(i\Delta \cdot \mathbf{r} - 1) | \Phi_j \right\rangle, \quad (13)$$

$$f_{II} = i\Delta^{-2} \sum_n \left\langle \psi_{C, k_e}^- | \exp(i\Delta \cdot \mathbf{r} - 1) | \Phi_n \right\rangle M_{nj} \left[\frac{J_{l-1}(\lambda)}{E_n - E_j - \omega} - \frac{J_{l+1}(\lambda)}{E_n - E_j + \omega} \right] \quad (14)$$

$$f_{III} = i\Delta^{-2} \sum_n \langle \Phi_n | \exp(i\Delta \cdot \mathbf{r} - 1) | \Phi_j \rangle M_{n,k_e}^* \left[\frac{J_{l-1}(\lambda)}{E_n - E_{k_e} + \omega} - \frac{J_{l+1}(\lambda)}{E_n - E_{k_e} - \omega} \right] - \frac{1}{2} \Delta_{\mathbf{k}_e} [J_{l-1}(\lambda) e^{i\gamma_{k_e}} - J_{l+1}(\lambda) e^{-i\gamma_{k_e}}] \langle \psi_{C,k_e}^- | \exp(i\Delta \cdot \mathbf{r}) | \Phi_j \rangle \quad (15)$$

Here, J_l is the Bessel function of order l , λ , argument of the Bessel function, which represents the quiver motion of the charged particle in the external CP laser field, and is given as ; [30]

$$\lambda^2 = \Delta_{k_s^2} + \Delta_{k_e^2} + \Delta_{k_i^2} + 2\Delta_{k_s k_e} \cos(\gamma_{k_s} - \gamma_{k_e}) - 2\Delta_{k_s k_i} \cos(\gamma_{k_s} - \gamma_{k_i}) - 2\Delta_{k_e k_i} \cos(\gamma_{k_e} - \gamma_{k_i}). \quad (16)$$

Within the framework of the first Born approximation, the triple differential cross section (TDCS) for the laser-assisted ($e, 2e$) process, accompanied by the absorption or emission of l photons, is written as

$$\frac{d^3 \sigma^{\text{B1},l}}{d\Omega_s d\Omega_e dE_e} = \frac{k_s k_e}{k_i} \left| f_{\text{ion}}^{\text{B1},l} \right|^2 \quad (17)$$

where the scattering amplitude $f_{\text{ion}}^{\text{B1},l}$ is defined in Eq. (12).

B. Twisted wave ($e, 2e$) on H-atom

The theoretical framework employed in the present study is based on the approach developed in our previous study [53] for the laser-assisted ($e, 2e$) process induced by twisted electron beams (TEB) for the linearly polarised laser-field. A twisted electron beam (TEB) can generally be represented as a coherent superposition of tilted plane waves [54]. And for the laser-assisted processes, this description extends to a superposition of Volkov states [55]. The transition matrix element takes the following form;

$$T_{fi}^{tw}(\boldsymbol{\varkappa}, \Delta, \mathbf{b}) = (-i)^{m_l} \sqrt{\frac{\boldsymbol{\varkappa}}{2\pi}} \int_0^{2\pi} \frac{d\phi_p}{2\pi} e^{im\phi_p - ik_{i\perp} \cdot \mathbf{b}} T_{fi}(\Delta), \quad (18)$$

here momentum transfer Δ depends on both longitudinal and transverse components of the incident beam [33]. Here $T_{fi}(\Delta)$ is given by equation (10). Here we compute the $T_{fi}(\Delta)$ for both the linearly and circularly polarised field. The transition amplitude in Eq. (18) explicitly depends on the impact parameter \mathbf{b} , which specifies the position of the target relative to the axis of the incident twisted electron beam. In this communication, we extend this formalism for the circularly polarized laser field. This description corresponds to an idealized microscopic scenario in which the scattering occurs from a single, spatially localized atom or molecule with a well-defined impact parameter. However, such conditions are difficult to realize experimentally, and better ionization target would be macroscopic target which typically consist of a large ensemble of randomly distributed atoms or molecules within the interaction region. For a macroscopic target, the averaged cross section $TDCS_{av}$ is given by [33]:

$$TDCS_{av} = \frac{1}{2\pi \cos \theta_p} \int_0^{2\pi} d\phi_p \frac{d^3 \sigma(\Delta)}{d\Omega_e d\Omega_s dE_e}. \quad (19)$$

From (19), we can see that the TDCS of a macroscopic target is independent on the projection of OAM (m_l) and the phase factor ($e^{im\phi}$). However, for such macroscopic targets we can recover the sensitivity of the TDCS to the OAM by treating the incident twisted electron beam as a coherent superposition of two twisted beams that share identical kinematic parameters but differ in their OAM projections. The wave function of such a superposed twisted electron beam is given as [54, 56] :

$$\Psi(\mathbf{r}) = c_1 \Psi_{m_{l_1}}(\mathbf{r}) + c_2 \Psi_{m_{l_2}}(\mathbf{r}) \quad (20)$$

Here $\Psi_{m_l}(\mathbf{r})$ is wavefunction of the TEB (given in equation (20) in Ref [53]), and the expansion coefficients c_n given as;

$$c_n = |c_n| e^{i\alpha_n}, \quad |c_1|^2 + |c_2|^2 = 1. \quad (21)$$

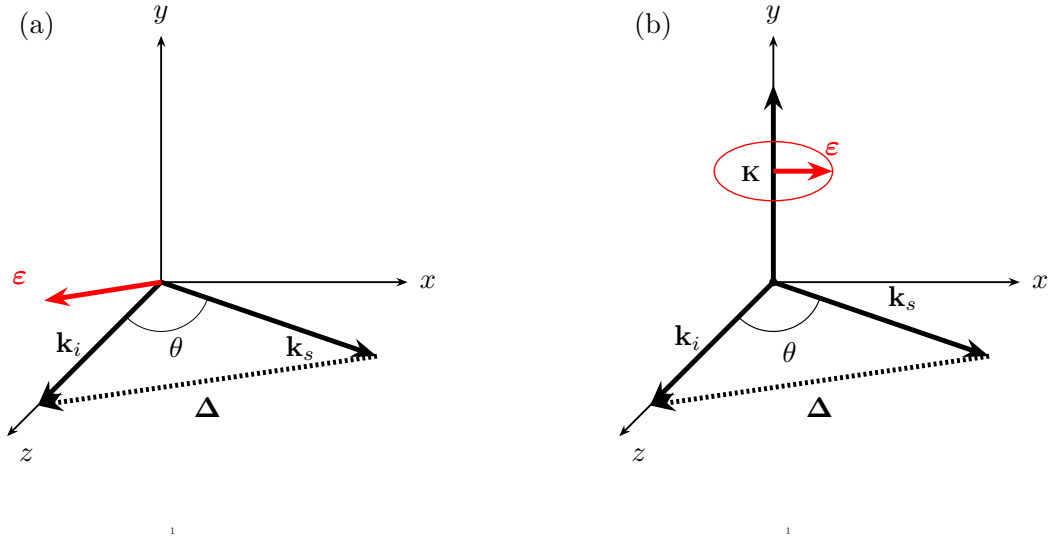


FIG. 1: Schematic illustration of the kinematic geometry for the laser-assisted (e,2e) reaction on atomic hydrogen. The incident electron momentum \mathbf{k}_i is aligned along the z -axis, and zx plane defines the scattering plane. (a) Configuration for linear polarization, where the electric field polarization vector ϵ is oriented parallel to the momentum transfer vector Δ . (b) Configuration for circular polarization (CP_Y), where the laser field propagates along the y -axis ($\mathbf{k} \parallel \hat{y}$), such that the electric field vector ϵ rotates within the zx scattering plane.

When the incident projectile is described by the coherent superposition state given in Eq. (20), the resulting TDCS depends on the interference of different OAMs and the relative phase between the two components. TDCS for the superposed twisted beam can be written in the following form;

$$\text{TDCS}_{\text{av}} = \frac{1}{2\pi \cos \theta_p} \int_0^{2\pi} d\phi_p G(\phi_p, \Delta m_l, \Delta\alpha) \frac{d^3\sigma(\Delta)}{d\Omega_s d\Omega_e dE_e}. \quad (22)$$

where $\Delta m_l = m_{l_2} - m_{l_1}$ is the difference in the OAM projections, $\Delta\alpha = \alpha_2 - \alpha_1$ is the difference in the phases of the twisted states, and the interference factor is given by $G(\phi_p, \Delta m, \Delta\alpha) = 1 + 2|c_1 c_2| \cos[(m_2 - m_1)(\phi_p - \frac{\pi}{2}) + \alpha_2 - \alpha_1]$.

III. RESULTS AND DISCUSSIONS

This study investigates the ionization of atomic hydrogen for the laser-assisted (e,2e) process on H-atom utilizing both incident plane waves and Twisted Electron Beams (TEB). As depicted in Figure 1, the analysis concentrates on two distinct polarization states: (a) linear polarization, where the polarization vector ϵ aligns parallel to the momentum transfer vector Δ and (b) circular polarization (CP_Y), characterized by the propagation along the Y-axis with the field polarized within the zx scattering plane.

A. Angular profile of TDCS for the laser-assisted (e,2e) process

Figure 2 shows the angular distribution of the triple differential cross section (TDCS) for laser-assisted ionization of atomic hydrogen in the Ehrhardt asymmetric coplanar geometry, calculated within the first Born approximation

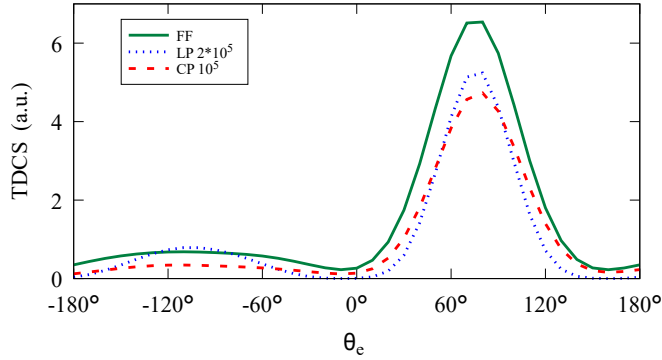


FIG. 2: Angular distributions of the Triple Differential Cross Section (TDCS) plotted against the ejected electron angle θ_e . The study compares three interaction regimes: the Field Free (FF) case (solid curve), laser-assisted collisions in a Linearly Polarized (LP) field (blue dotted curve), with the polarization vector parallel to the momentum transfer direction; and laser-assisted collisions in a Circularly Polarized (CP_Y) field (red dashed curve), with the polarization vector aligned along the y -axis within the scattering (zx) plane. Kinematic parameters are fixed at incident energy $E_i = 600$ eV, ejected energy $E_e = 5$ eV, and scattering angle $\theta_s = 4^\circ$. Laser parameters correspond to the absorption of $l = 1$ photon with field strength $\varepsilon = 10^6$ V/m and photon energy $\hbar\omega = 1.17$ eV. The specific scaling factors are indicated in the panel to compare with the field free results.

for an incident electron energy $E_i = 600$ eV, scattering angle $\theta_s = 4^\circ$, and fixed ejected electron energy $E_e = 5$ eV, as a function of the ejection angle θ_e . The laser field corresponds to single-photon absorption ($l = 1$) with field strength $\varepsilon = 10^6$ V/m and photon energy $\hbar\omega = 1.17$ eV. Results obtained for circular polarization (CP_Y) are compared with those for linear polarization with the polarization vector parallel to the momentum transfer direction ($\varepsilon \parallel \Delta$). The calculations reproduce the characteristic binary and recoil peak structures reported previously [31], with a dominant binary peak and a reduced, broadened recoil peak. Moreover, the TDCS magnitude for circular polarization is found to be approximately twice that obtained for the corresponding linear polarization case, in agreement with earlier theoretical predictions [30]. The overall agreement with the available data confirms the validity of the present approach in the high-impact-energy regime, where exchange effects are negligible and laser-induced modifications dominate over higher-order contributions.

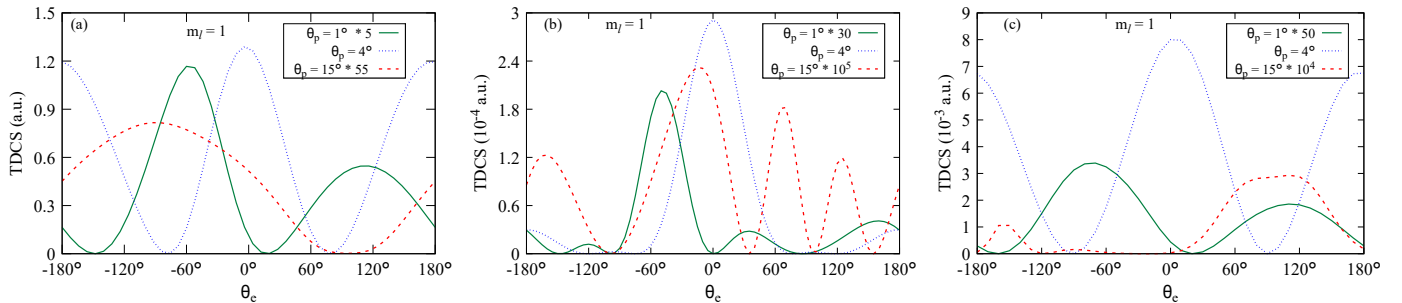


FIG. 3: Angular distributions of the Triple Differential Cross Section (TDCS) for orbital angular momentum $m_l = 1$, plotted against the ejected electron angle θ_e . The study compares three interaction regimes: (a) the Field Free (FF) case; (b) laser-assisted collisions in a Linearly Polarized (LP) field, with the polarization vector parallel to the momentum transfer direction; and (c) laser-assisted collisions in a Circularly Polarized (CP_Y) field, with the polarization vector aligned along the y -axis within the scattering (zx) plane. The curves denote opening angles of $\theta_p = 1^\circ$ (solid green), $\theta_p = 4^\circ$ (blue dotted), and $\theta_p = 15^\circ$ (red dashed). Kinematic parameters are same as the fig 1.

In figure 3 we present the TDCS for TEB collision as a function of ejected electron angle θ_e for the kinematics as figure 2 keeping OAM $m_l = 1$ and selecting different θ_p as mentioned in the graph. In figures 3(a), (b), and (c), we illustrate the variations of the TDCS for opening angle $\theta_p = 1^\circ$ (solid green curve), 4° (blue dotted curve), and 15° (red dashed curve). Here we compare the results for field free case (FF), linearly polarised field (LP) and circularly polarised laser field (CP_Y). In a quantitative comparison of the TDCS magnitudes for all three scenarios (FF, LP, and CP_Y), we observed that the FF process yields the maximum amplitude. When a laser field is introduced, a significant

suppression is observed: the CP_Y field attenuates the TDCS magnitude by approximately two orders of magnitude relative to the FF study. This effect is even more pronounced in the linearly polarized (LP) case, where the cross-section diminishes by roughly three orders of magnitude (see figure 3(a),(b) and (c)). These findings demonstrate that the ionization probability is also highly sensitive to the specific polarization state, similar to the plane wave case in the figure 2.

A comparative analysis of the angular distribution of TDCS reveals that the observed behavior is highly sensitive to the relation between the scattering angle θ_s and the opening angle θ_p of the twisted electron beam. We observe from all the plots that TDCS exhibit the maximum magnitude for $\theta_s = \theta_p$, relative to the kinematics when $\theta_s \neq \theta_p$. In particular, for the specific kinematic condition $\theta_s = \theta_p$, the angular distribution obtained in the CP_Y case seems to follow roughly similar patterns that of the FF process. Here we observed two peak structures, a forward peak in the direction $\theta_e = 0^\circ$ and backward peak in the $\theta_e = \pm 180^\circ$ direction (see blue dotted curve in figure 3(a) and (c)). In contrast, for the LP field, the backward peak in the $\theta_e = \pm 180^\circ$ is suppressed, and a prominent forward peak in the direction $\theta_e = 0^\circ$ is observed (see blue dotted curve in figure 3(b)). The similarity between the CP_Y and FF angular distributions is not a general feature. When $\theta_s \neq \theta_p$, the angular distribution for the CP_Y and the FF case deviates significantly from one another (see the green solid and red dashed curves in figure 3(a) and (c)). This similarity between the FF and CP_Y angular behavior observed for $\theta_s = \theta_p = 4^\circ$ (in this study) may be understood in terms of an effective kinematic symmetry associated with the momentum structure of the twisted electron beam. A twisted beam consists of a coherent superposition of plane-wave components whose momenta lie on a cone defined by the opening angle θ_p . When the scattering angle is equal to the opening angle, contributions from the dominant transverse momentum components of the incident beam symmetrically enter the scattering process. Since a circularly polarized laser field does not introduce a fixed direction in the scattering plane, this effective symmetry is preserved, leading to an angular distribution that closely resembles the field-free case.

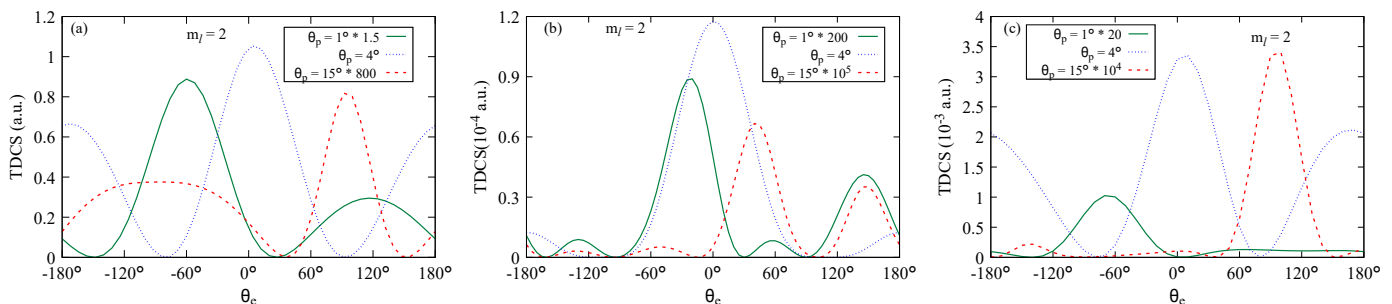


FIG. 4: Kinematics is same as figure 3 except the $m_l = 2$

Figure 4 presents the TDCS for $m_l = 2$, with the same kinematics employed in figure 3, except OAM ($m_l = 2$). Here we observe that with the increment of OAM the magnitude of the TDCS decreases.

In particular, compared to the field-free case, the magnitude of TDCS is suppressed by two orders of magnitude in the presence of a CP_Y field and by about three orders of magnitude for the LP field (LP). For the specific kinematic condition $\theta_s = \theta_p = 4^\circ$, the angular distributions for the FF and CP_Y cases again exhibit similar features, characterized by the presence of both forward and backward emission peaks. This behavior contrasts with that observed for the LP case, where the backward emission is strongly suppressed and the TDCS is dominated by a forward peak. This trend is consistent with the behavior observed for the $m_l = 1$ and confirms that the similarity between the FF and CP_Y cases persists at $m_l = 2$ only for this specific geometrical condition.

When the scattering angle differs from the opening angle, namely for $\theta_p = 1^\circ$ and 15° , the angular distributions for the three scenarios (FF, LP, and CP_Y) differ significantly, as shown in Figs. 4(a)–(c) (see green solid and red dashed curves). In the field-free case [Fig. 4(a)], the TDCS exhibits two distinct peaks at $\theta_e = -60^\circ$ and 120° for $\theta_p = 1^\circ$ (see green solid curve), whereas for $\theta_p = 15^\circ$ the distribution is characterized by a pronounced peak near $\theta_e = 90^\circ$ together with a broad structure extending from $\theta_e = 0^\circ$ to 180° (see red dashed curve).

In contrast, the laser-assisted cases display a simpler angular behavior. For both LP and CP_Y , the TDCS is dominated by a single main peak when $\theta_s \neq \theta_p$. In the LP case [Fig. 4(b)], the TDCS exhibits a prominent peak located near $\theta_e = -30^\circ$ for $\theta_p = 1^\circ$ (see green solid curve) and near $\theta_e = 40^\circ$ for $\theta_p = 15^\circ$, accompanied by weaker subsidiary lobes (see red dashed curve). For the circularly polarized case CP_Y (Fig. 4(c)), a similar single-peak structure is observed, but without the additional small lobes present in the LP distributions. At $\theta_p = 1^\circ$, the TDCS is characterized by a dominant peak near $\theta_e = -60^\circ$ (see green solid curve), while for $\theta_p = 15^\circ$ the main peak shifts to $\theta_e = 90^\circ$ (see red dashed curve). The absence of secondary lobes in the CP_Y case further emphasizes the role of laser polarization in determining the detailed angular structure of the TDCS.

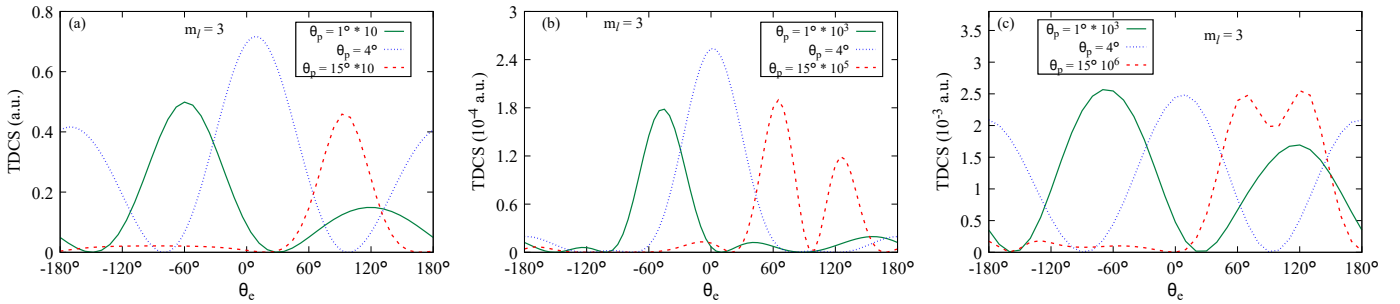


FIG. 5: Kinematics is same as figure 3 except the $m_l = 3$

An analysis of the TDCS for higher OAM's $m_l = 3$ and 4, presented in Figs. 5 and 6 reveal a further reduction in magnitude compared to those obtained for $m_l = 1$ and 2 shown in Figs. 3 and 4. This progressive decrease in the TDCS with increasing OAM is consistent with the general trend observed throughout the present study, indicating that higher OAM states of the twisted projectile lead to a reduced ionization probability. Regarding the angular distribution, we observe that for the kinematic condition $\theta_s = \theta_p$, the TDCS profiles for $m_l = 3$ and 4 exhibit qualitative features similar to those of $m_l = 1$ and 2. This angular distribution similarity persists across all three interaction regimes investigated: Field-Free (FF), Linear Polarization (LP), and Circular Polarization (CP_Y). This observation confirms that the geometric symmetry between the scattering angle and the opening angle (i.e. $\theta_s = \theta_p$) plays a dominant role in shaping the angular structure of the TDCS.

In the FF scenario, a detailed comparison shows that the angular distribution remains similar at small projectile scattering angles ($\theta_p = 1^\circ$ and 4°) for all OAM (m_l) values considered in this work. However, significant deviations arise when the opening angle is increased to $\theta_p = 15^\circ$, indicating an enhanced sensitivity to the transverse momentum content of the twisted beam at larger opening angles. Upon the introduction of the laser field, the scattering dynamics exhibit a distinct dependence on the OAM's odd-even nature. For the kinematic case $\theta_s = \theta_p$, the angular distribution remains uniform across all studied OAM values for LP and CP_Y polarization conditions. In contrast, when $\theta_p = 1^\circ$, a clear dependence on the nature of the OAM becomes apparent in the laser-assisted cases. Odd OAM values ($m_l = 1$ and 3) yield nearly identical angular distributions, characterized by a dominant peak around $\theta_e = 50^\circ$. In contrast, even OAM values ($m_l = 2$ and 4) exhibit a peak shifted toward $\theta_e = 30^\circ$, accompanied by small lobes, as illustrated by the solid green curves in Figs. 3–6. This odd–even character of the OAM-dependent behavior highlights the role of the phase structure of the twisted projectile in the presence of the laser field. Similar to the FF case, this odd–even symmetry breaks down at $\theta_p = 15^\circ$, where the angular distribution varies differently with the OAM number (red dashed curves in Figs. 3–6). The angular distributions thus show a clear dependence on the nature of m_l , where odd values exhibit similar profiles that differ from those corresponding to even values. These results suggest that the combined effects of the laser polarization, the orbital angular momentum of the twisted electron beam, and the beam opening angle influence the angular structure of the TDCS.

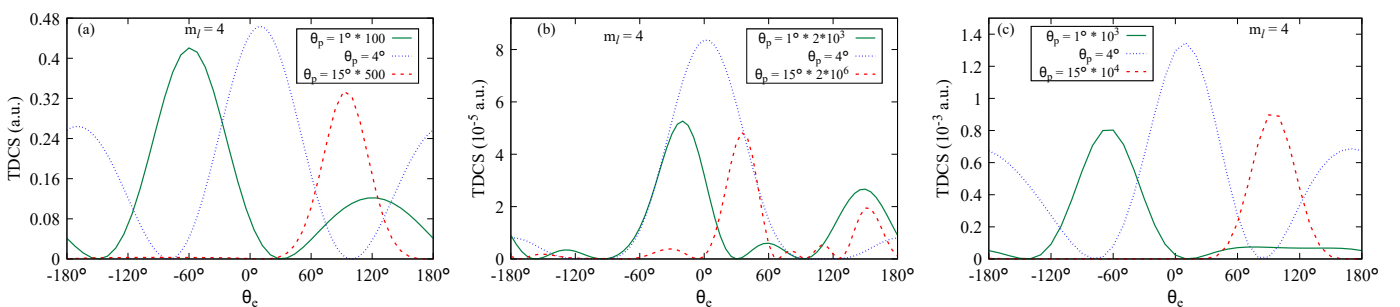


FIG. 6: Same as figure 3 except $m_l = 4$

B. Triple Differential Cross-Sections for macroscopic Target

Here we present the angular distribution $TDCS_{av}$ as a function of θ_e for the macroscopic target, which represents the realistic experimental scenario of twisted free electrons interacting with a macroscopic target. Figure 7 illustrates $TDCS_{av}$ for three scenarios (a) for field free FF, (b) for laser-assisted with linearly polarised laser-field LP and (c) for circularly polarised laser field CP_Y . $TDCS_{av}$ is calculated at the same kinematics employed in the Figure 3. Here we like to retreat that the $TDCS_{av}$ only depends on opening angle and independent on OAM. The opening angles considered here are as follows $\theta_p = 1^\circ$, 4° and 15° , and the corresponding $TDCS_{av}$ angular profiles are represented by green solid curve, blue dotted curve and red dashed curve respectively. A detailed comparison of the, $TDCS_{av}$, for the three cases considered in this work—namely the field-free (FF) case [Fig. 7(a)], linear polarization (LP) [Fig. 7(b)], and circular polarization (CP_Y) [Fig. 7(c)]—reveals that the presence of the laser field significantly modifies both the magnitude and the angular distribution of $TDCS_{av}$. For the field-free case at an opening angle $\theta_p = 1^\circ$, two pronounced peaks are observed in the vicinity of the perpendicular emission directions, $\theta_e = 90^\circ$ and 270° . This symmetry is altered when the laser field is introduced. In the LP case, the angular distribution exhibits two shifted maxima located at $\theta_e = 120^\circ$ and 310° . In contrast, for the CP_Y configuration, the distribution is dominated by a single peak centered around $\theta_e = 180^\circ$, accompanied by additional weaker side peaks. These observations clearly demonstrate that the polarization state of the laser field plays a crucial role in reshaping the ionization dynamics and the angular emission pattern of electrons from macroscopic targets. From our results we also observed that the peak value of the $TDCS_{av}$, decreases as the opening angle of the twisted electron beam increases to $\theta_p = 15^\circ$ (a significant reduction in the magnitude can be seen from figure 7 as red dashed curve is scaled up by different factor for three different case for better comparison). This trend is consistent with our earlier findings obtained from the TDCS calculations in figures 3-6. This reduction in the magnitude can be understood as follows; the opening

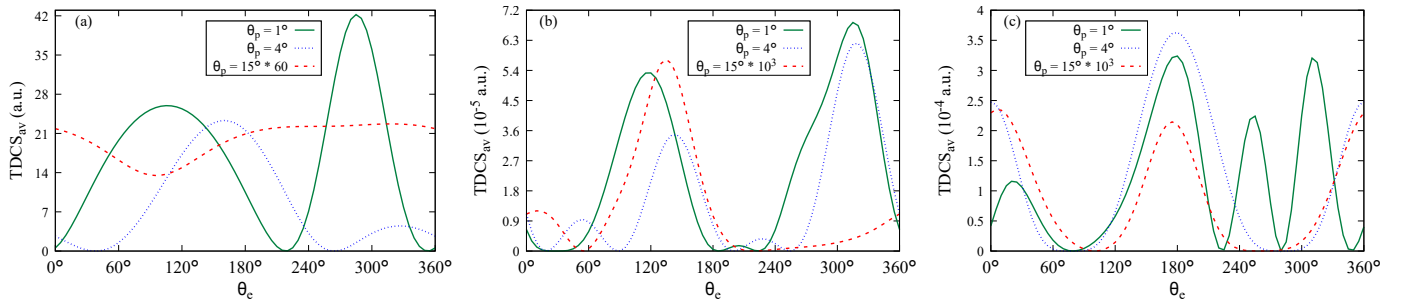


FIG. 7: Triple Differential Cross Section of macroscopic target ($TDCS_{av}$) for hydrogen atoms by TEB, plotted against the ejected electron angle θ_e . The study compares three interaction regimes: (a) the Field Free (FF) case; (b) laser-assisted collisions in a Linearly Polarized (LP) field, with the polarization vector parallel to the momentum transfer direction; and (c) laser-assisted collisions in a Circularly Polarized (CP_Y) field, with the polarization vector aligned along the y -axis within the scattering (zx) plane. The curves denote opening angles of $\theta_p = 1^\circ$ (solid green), $\theta_p = 4^\circ$ (blue dotted), and $\theta_p = 15^\circ$ (red dashed). The kinematics employed is same as of figure 3. The specific scaling factors are indicated in the respective panels.

angle θ_p determines how the projectile's total momentum is divided into transverse ($k_\perp = k \sin \theta_p$) and longitudinal ($k_z = k \cos \theta_p$) components. Increasing θ_p naturally increases the transverse momentum while reducing the forward (longitudinal) momentum. Consequently, the effective electron flux available for ionization in the scattering direction plane. Furthermore, a larger opening angle expands the cone of plane-wave components in momentum space. This combination of reduced longitudinal momentum leads to a systematic reduction in the magnitude of $TDCS_{av}$ and TDCS as the opening angle increases.

C. Triple differential cross-section for superposition of two Bessel Beams

Figures 8–10 present the TDCS for the coherent superposition of two Bessel beams for relative phases $\alpha = 0^\circ$, 60° , and 90° . The use of a superimposed Bessel-beam configuration provides a realistic framework for examining the influence of the OAM projection Δm_l on the ($e, 2e$) process. The TDCS is evaluated for $\Delta m_l = 1, 2, 3$, and 4, and are represented by the green solid, blue dotted, red dashed, and purple dash-dotted curves, respectively. The results are shown for (a) the field-free case (FF), (b) a linearly polarized laser field (LP), and (c) a circularly polarized laser field (CP_Y), under the same kinematical conditions as those employed in Figure 7.

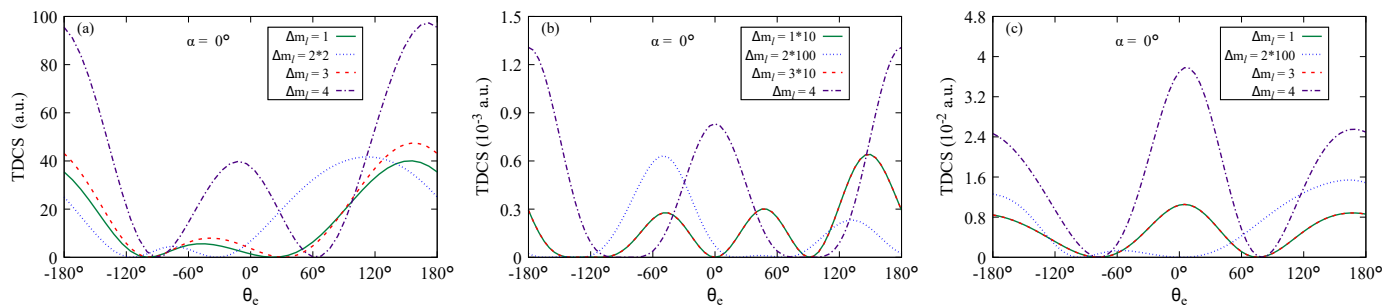


FIG. 8: Triple Differential Cross Section (TDCS) for hydrogen atoms by coherent superposition of two Bessel beams for phase difference $\alpha = 0^\circ$. The study compares three interaction regimes: (a) the Field Free (FF) case; (b) laser-assisted collisions in a Linearly Polarized (LP) field, and (c) laser-assisted collisions in a Circularly Polarized (CP_Y) field. Kinematics employed is same as of figure 3. The different OAM projections for which calculations are performed are mention in the penal.

For $\alpha = 0^\circ$, corresponding to the case where the two incident twisted electron beams are in phase, the field-free results indicate that the OAM projections $\Delta m_l = 1, 2$, and 3 exhibit nearly identical angular distributions with pronounced peaks around $\theta_e = \pm 180^\circ$, while the $\Delta m_l = 2$ yields the smallest TDCS magnitude. In contrast, the $\Delta m_l = 4$ contribution displays the largest TDCS, characterized by a two-peak structure consisting of a forward peak near $\theta_e = 15^\circ$ and a n dominant backward peak at $\theta_e = \pm 180^\circ$.

In the presence of the laser field, a distinctive behavior emerges when the two Bessel beams are in phase. For both the LP and CP_Y laser-assisted collisions, the odd OAM projections $\Delta m_l = 1$ and 3 produce identical angular distributions of the TDCS, as evidenced by the complete overlap of the corresponding curves (green solid and red dashed curves) in Figures 8(b) and 8(c). This indicates that, under coherent in-phase superposition, the laser-assisted dynamics become insensitive to the odd value of Δm_l . However, despite this similarity between $\Delta m_l = 1$ and 3 within each polarization scheme, the angular profiles of the LP and CP_Y configurations differs markedly (see green solid and red-dashed curve in Figures 8(b) and (c)), reflecting the distinct symmetry and coupling characteristics associated with linear and circular laser polarizations. Furthermore, the even OAM projections reveal a significant dependence on the specific laser polarization state, highlighting a clear departure from the behavior of the odd projections. In the LP configuration, $\Delta m_l = 2$ distribution (blue dotted curve) is characterized by a distinct two-peak structure located at $\theta_e = -60^\circ$ and 120° . In contrast, the $\Delta m_l = 4$ contribution (purple dash-dotted curve) exhibits both forward and backward peaks at $\theta_e = 0^\circ$ and $\theta_e = \pm 180^\circ$, respectively, with the backward peak being dominant over the forward emission. The CP_Y case presents a markedly different trend. For $\Delta m_l = 2$, the angular distribution is restricted primarily to a single backward peak, suppressing the forward emission seen in the LP case. Meanwhile, for $\Delta m_l = 4$ TDCS_{av} displays a dual-peak structure exhibiting both forward and backward components. Notably, in direct contrast to the LP results, the forward peak in the CP_Y configuration dominates the backward emission. This inversion of peak dominance indicates that the circular polarization enhances forward scattering for higher-order OAM transfers, a feature that could be instrumental in controlling ejected electron emission directions in twisted-beam experiments.

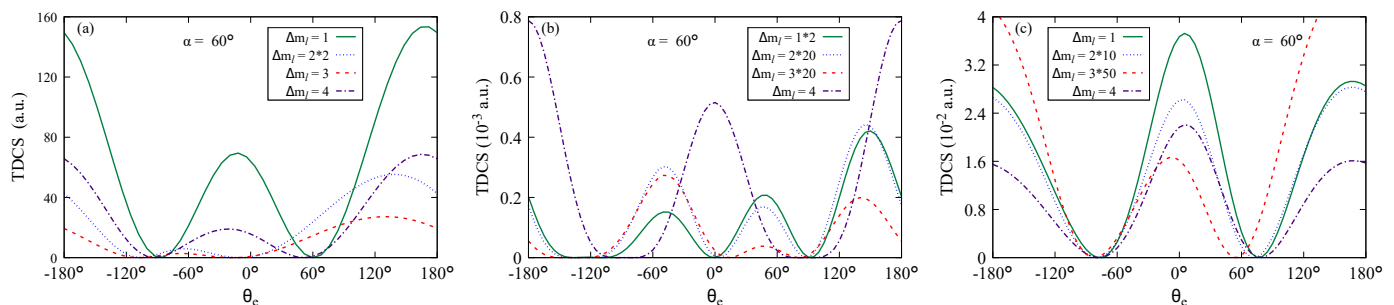


FIG. 9: Same as figure 8 except phase factor $\alpha = 60^\circ$

As the relative phase between the two Bessel beams is increased from $\alpha = 0^\circ$ to 60° and 90° , the TDCS exhibits a phase sensitivity that depends on both the OAM projection and the laser polarization. The phase variation (from $\alpha = 0^\circ$ to $\alpha = 60^\circ$ and $\alpha = 90^\circ$) breaks the similarity of the TDCS observed for odd OAM projections at $\alpha = 0^\circ$ (see green solid and red dashed curves in Figure 9(b) and (c)). In the LP laser-assisted case, the angular distributions

for $\Delta m_l = 1$ and 3, which are identical at $\alpha = 0^\circ$, become distinct for $\alpha = 60^\circ$ and 90° , while the $\Delta m_l = 1$ and 2 channels exhibit similar angular profiles differing primarily in magnitude. This indicates that, for LP scenario, the phase variation modifies the interference between OAM projections, leading to a redistribution of the TDCS without significantly altering the overall emission distribution. For the CP_Y configuration, the phase dependence is more intricate. For $\alpha = 60^\circ$, the angular distributions corresponding to the $\Delta m_l = 1, 2, 3$ and 4 values remain broadly similar, with the primary differences appearing in the magnitude of the TDCS rather than in the peak positions. When the phase difference is increased to $\alpha = 90^\circ$, a stronger dependence on the Δm_l becomes evident, with the $\Delta m_l = 3$ component exhibiting a noticeable modification in both magnitude and angular profile, while the $\Delta m_l = 1, 2$, and 4 components remain comparatively closer to their distributions at $\alpha = 60^\circ$. This behavior indicates that increasing the phase difference enhances the interference between the twisted components, leading to a more pronounced redistribution of the TDCS. These observations demonstrate that the relative phase between the superposed twisted beams acts as an additional parameter for controlling the angular distribution of the ionization process.

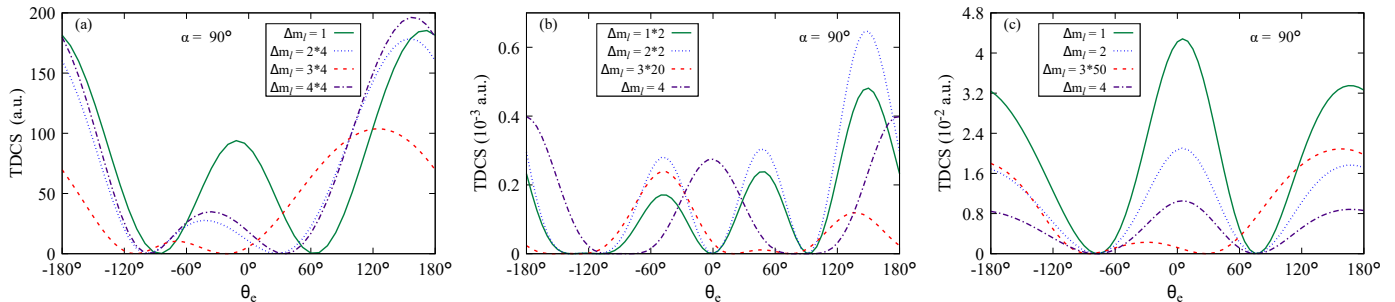


FIG. 10: Same as 8 except phase factor $\alpha = 90^\circ$.

IV. CONCLUSION

We have investigated laser-assisted (e,2e) ionization of hydrogen atom by twisted electron beams, for both linearly and circularly polarized laser fields. Our work focused on the roles of laser polarization, orbital angular momentum (OAM), beam opening angle, and coherent beam superposition on the angular distribution of TDCS and TDCS_{av}. Within the one-photon absorption regime, we find that the presence of a laser field strongly suppresses the triple differential cross section (TDCS), with linear polarization producing a significantly larger reduction than that for the circular polarization. A key result is the emergence of an effective kinematic symmetry when the projectile scattering angle (θ_s) equals the opening angle (θ_p) of the twisted electron beam. Under this condition, the angular distribution in the circularly polarized case closely resembles that of the field-free process, while pronounced deviations occur when this geometric relation is not satisfied ($\theta_s \neq \theta_p$). Increasing the OAM of the TEB projectile leads to a systematic decrease in the TDCS magnitude, although the angular distribution remains largely unchanged. For laser-assisted collisions, the angular distributions exhibit a clear dependence on the odd and even nature of the OAM at small opening angles ($\theta_p = 1^\circ$ and 4°), reflecting the phase structure of the twisted electron beam. This behavior disappears at comparatively large opening angle $\theta_p = 15^\circ$, where the distributions become strongly OAM dependent. For the coherent superposition of two Bessel beams, the in-phase configuration ($\alpha = 0^\circ$) yields identical TDCS distributions for the odd OAM projections. While for a non-zero phase difference ($\alpha = 60^\circ$ and 90°) breaks this similarity, and the resulting distributions depend on both the OAM projection and the laser polarization. The effect is more substantial for circular polarization, with greater sensitivity to the relative phase between the beams. Our results demonstrate that laser polarization, beam geometry, and OAM provide powerful and complementary control parameters for tailoring electron-impact ionization dynamics with twisted electron beams.

-
- [1] F. Byron Jr and C. J. Joachain, *Physics reports* **179**, 211 (1989).
 - [2] K. Bartschat and M. J. Kushner, *Proceedings of the National Academy of Sciences* **113**, 7034 (2016).
 - [3] L. G. Christophorou and J. K. Olthoff, *Journal of Physical and Chemical Reference Data* **29**, 330 (2000).
 - [4] E. Shalenov, K. Dzhumagulova, and T. Ramazanov, *Physics of Plasmas* **24** (2017).

- [5] M. A. de Avillez, M. Guerra, J. P. Santos, and D. Breitschwerdt, *Astronomy Astrophysics* **631**, A42 (2019).
- [6] H. Ehrhardt, K. Jung, G. Knoth, and P. Schlemmer, *Zeitschrift für Physik D Atoms, Molecules and Clusters* **1**, 32 (1986).
- [7] H. Ehrhardt, M. Schulz, T. Tekaas, and K. Willmann, *Physical review letters* **22**, 89 (1969).
- [8] H. Ehrhardt, M. Fischer, K. Jung, F. Byron Jr, C. Joachain, and B. Piraux, *Physical Review Letters* **48**, 1807 (1982).
- [9] F. Ehlötzky, A. Jaro, and J. Kami ski, *Physics reports* **297**, 153 (1998).
- [10] C. Hohl, A. Dorn, B. Najjari, D. Fischer, C. Schroter, and J. Ullrich, *Physical review letters* **94**, 153201 (2005).
- [11] C. Hohl, A. Dorn, B. Najjari, D. Fischer, C. Schrter, and J. Ullrich, *Journal of Electron Spectroscopy and Related Phenomena* **161**, 177 (2007).
- [12] M. H. Mittleman, *Introduction to the theory of laser atom interactions* (Springer Science Business Media, 2013).
- [13] P. Francken and C. Joachain, *Journal of the Optical Society of America B* **7**, 563 (1990).
- [14] F. Ehlötzky, *Physics Reports* **345**, 264 (2001).
- [15] M. Mohan and P. Chand, *Physics Letters A* **65**, 401 (1978), ISSN 9601.
- [16] P. Cavaliere, G. Ferrante, and C. Leone, *Journal of Physics B: Atomic and Molecular Physics* **13**, 4495 (1980).
- [17] S. K. Mandal and A. Ghosh, *Physical Review A* **30**, 2759 (1984).
- [18] P. Cavaliere, C. Leone, R. Zangara, and G. Ferrante, *Physical Review A* **24**, 910 (1981).
- [19] J. Banerji and M. Mittleman, *Journal of Physics B: Atomic and Molecular Physics* **14**, 3717 (1981).
- [20] R. Zangara, P. Cavaliere, C. Leone, and G. Ferrante, *Journal of Physics B: Atomic and Molecular Physics* **15**, 3881 (1982).
- [21] M. Zarcone, D. Moores, and M. McDowell, *Journal of Physics B: Atomic and Molecular Physics* **16**, L11 (1983).
- [22] C. Joachain, P. Francken, A. Maquet, P. Martin, and V. Veniard, *Physical review letters* **61**, 165 (1988).
- [23] P. Martin, V. Veniard, A. Maquet, P. Francken, and C. Joachain, *Physical Review A* **39**, 6178 (1989).
- [24] S. Ghosh Deb, S. Roy, and C. Sinha, *The European Physical Journal D* **55**, 600 (2009).
- [25] S. M. Li, J. Berakdar, S. T. Zhang, and J. Chen, *Journal of Electron Spectroscopy and Related Phenomena* **161**, 190 (2007).
- [26] S. Li, J. Berakdar, S. Zhang, and J. Chen, *Journal of Physics B Atomic, Molecular and Optical Physics* **38**, 1291 (2005).
- [27] A. Chattopadhyay and C. Sinha, *Physical Review A Atomic, Molecular, and Optical Physics* **72**, 053406 (2005).
- [28] H. W. van der Hart and L. Feng, *Journal of Physics B: Atomic, Molecular and Optical Physics* **34**, L601 (2001).
- [29] J. Sanz and H. J. Kull, *Physical Review A* **60**, 3896 (1999).
- [30] A. Makhoute, D. Khalil, A. Maquet, C. Joachain, and R. Taieb, *Journal of Physics B Atomic, Molecular and Optical Physics* **32**, 3255 (1999).
- [31] R. Taieb, V. Veniard, A. Maquet, S. Vucic, and R. Potvliege, *Journal of Physics B Atomic, Molecular and Optical Physics* **24**, 3229 (1991).
- [32] D. Khalil, A. Maquet, R. Taieb, C. Joachain, and A. Makhoute, *Physical Review A* **56**, 4918 (1997).
- [33] A. Harris, A. Plumadore, and Z. Smozhanyk, *Journal of Physics B Atomic, Molecular and Optical Physics* **52**, 094001 (2019).
- [34] A. Harris, *Physical Review A* **108**, 062810 (2023).
- [35] N. Dhankhar and R. Choubisa, *Journal of Physics B Atomic, Molecular and Optical Physics* **54**, 015203 (2020).
- [36] N. Dhankhar and R. Choubisa, *Physical Review A* **105**, 062801 (2022).
- [37] N. Dhankhar, S. Banerjee, and R. Choubisa, *Journal of Physics B Atomic, Molecular and Optical Physics* **55**, 165202 (2022).
- [38] N. Dhankhar, Neha, and R. Choubisa, *Atoms* **11**, 82 (2023).
- [39] A. Mandal, N. Dhankhar, D. Sebilliau, and R. Choubisa, *Physical Review A* **104**, 052818 (2021).
- [40] N. Dhankhar, A. Mandal, and R. Choubisa, *Journal of Physics B Atomic, Molecular and Optical Physics* **53**, 155203 (2020).
- [41] R. Van Boxem, B. Partoens, and J. Verbeeck, *Physical Review A* **89**, 032715 (2014).
- [42] R. Van Boxem, B. Partoens, and J. Verbeeck, *Physical Review A* **91**, 032703 (2015).
- [43] M. Uchida and A. Tonomura, *nature* **464**, 739 (2010).
- [44] S. Lloyd, M. Babiker, G. Thirunavukkarasu, and J. Yuan, *Reviews of Modern Physics* **89**, 035004 (2017).
- [45] K. Y. Bliokh, I. P. Ivanov, G. Guzzinati, L. Clark, R. Van Boxem, A. Beche, R. Juchtmans, M. A. Alonso, P. Schattschneider, F. Nori, et al., *Physics Reports* **690**, 70 (2017).
- [46] H. Larocque, I. Kaminer, V. Grillo, G. Leuchs, M. J. Padgett, R. W. Boyd, M. Segev, and E. Karimi, *Contemporary Physics* **59**, 126 (2018).
- [47] J. Verbeeck, H. Tian, and P. Schattschneider, *Nature* **467**, 304 (2010).
- [48] B. J. McMorran, A. Agrawal, I. M. Anderson, A. A. Herzing, H. J. Lezec, J. J. McClelland, and J. Unguris, *science* **331**, 195 (2011).
- [49] A. O'neil, I. MacVicar, L. Allen, and M. Padgett, *Physical review letters* **88**, 053601 (2002).
- [50] S. Furfapter, A. Jesacher, S. Bernet, and M. Ritsch Marte, *Optics Express* **13**, 694 (2005).
- [51] G. Berkhout and M. Beijersbergen, *Journal of Optics A: Pure and Applied Optics* **11**, 094021 (2009).
- [52] S. Gsmeider and J. M. Rost, *Physical Review A* **100**, 043408 (2019).
- [53] Neha, N. Dhankhar, R. S. Pinto, and R. Choubisa, *Journal of Physics B: Atomic, Molecular and Optical Physics* **57**, 095202 (2024).
- [54] V. Serbo, I. Ivanov, S. Fritzsche, D. Seipt, and A. Surzhykov, *Physical Review A* **92**, 012705 (2015).
- [55] D. V. Karlovets, *Physical Review A Atomic, Molecular, and Optical Physics* **86**, 062102 (2012).
- [56] D. V. Karlovets, G. Kotkin, V. Serbo, and A. Surzhykov, *Physical Review A* **95**, 032703 (2017).